Chapter 5

Role of Water Molecule(s) of Crystallization in the Modulation of Solubility and Membrane Permeability of Molecular Salts of Trimethoprim

5.1 Abstract

The antibiotic drug trimethoprim (TRM) is mainly used for the treatment of urinary tract infections. It is a BCS class II drug with extremely low solubility which lowers its bioavailability followed by affecting its efficacy. Employing crystal engineering principles, molecular salts of TRM are formulated through mechanochemical liquid-assisted grinding with six isomeric dihydroxybenzoic acids (DHBA) as coformers. The product materials were analyzed using FT-IR, DSC, TGA, PXRD, and single crystal X-RD. The crystallization of the drug with 24-DHBA, 34-DHBA, and 35-DHBA coformers results in the formation of hydrated salts with different ratios of water molecules of crystallization. The remaining coformers result in anhydrous forms with the drug. All products are put through solubility and membrane permeability measurements in various pH to study the performance of the drug. Inclusion of water molecules of crystallization in the multicomponent solids, i.e., TRM-24, TRM-34, and TRM-35 colossal impact in their properties as compared to that of the anhydrous salts, i.e. TRM-23, TRM-25, and TRM-26. The modification of the intermolecular interactions in the drug through the salt formation with coformers resulted in the enhancement of solubility and membrane permeability.

5.2 Introduction

Trimethoprim is an antifolate drug that is used to treat urinary tract infections (bladder infections) and pneumonia. It selectively inhibits the dihydrofolate reductase enzyme formation in bacteria without interfering dihydrofolate reductase of mammalian [1–3]. The drug is categorized under BCS class II (low soluble and highly permeable) [4]. The absorption of the drug in the gastrointestinal tract is low due to extremely low solubility in the aqueous media which in turn causes a decrease in the concentration at the target site and significantly hampers its efficiency [5]. Optimization method like solid dispersion was used to enhance the solubility and in vivo bioavailability of the drug trimethoprim [6]. Because of stability issues during storage, this method is not favorable for drug formulation in the pharmaceutical industry. Formulation of multicomponent solids such as

cocrystals and salts has become a powerful method to enhance drug properties by changing the intermolecular interactions [7,8]. Supramolecular synthons play a key role in the design and formation of molecular solids [9,10]. The modifying agents (coformers) are selected based on the synthon compatibility with the drug molecule. Regarding the modification of different physicochemical properties of drug molecules, several articles which demonstrate plentiful ideas and understanding of exactly how the drug efficacy changes/increases with the formation of cocrystals/salts have been published [11–19].

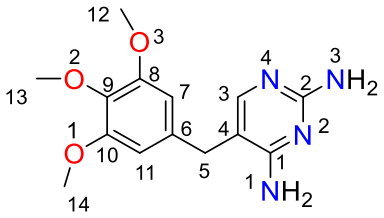

Scheme 5.1 Molecular structure of drug trimethoprim (TRM)

In this work, we improved the solubility and permeation parameters of the trimethoprim through multicomponent solid formulations using crystal engineering techniques. Most of the studies reported on the multicomponent crystals of trimethoprim with various coformers focus on structural analysis to understand the hydrogen bonding patterns between the drug and the coformers [20–27]. Only a few cocrystals/salts of trimethoprim with improved physicochemical properties and antimicrobial activity have been reported in the literature and listed in Table 5.1 [28–31]. For instance, multidrug cocrystals of trimethoprim-nitrofurantoin displayed higher solubility and better antimicrobial activity against gram-negative bacteria as compared to that of the individual components [28]. Ghosh et al. have demonstrated that there is an enhancement in the solubility of the salts of trimethoprim with fenamic acids in comparison to the pure individual starting materials [29]. Zaini et al. have also reported enhanced solubility and antibacterial activity for the salt of the drug with malic acid [30]. The salt of the drug with nicotinamide improved its solubility as compared to the pure drug [31]. In this chapter, we present six molecular salts of the antibiotic drug trimethoprim that show higher solubility and membrane permeation behaviors than the parent drug molecule. It was observed that hydrated salts demonstrated better physicochemical properties than the anhydrous salts of trimethoprim. The scope of this study is to investigate how the solubility and permeability of these molecular salts tuned in different pH conditions by variation of isomeric positions of phenolic OH groups of the coformers and inclusion of water molecules of crystallization.

Table 5.1 Reported cocrystals/salts of TRM with improved physicochemical properties.

Coformers	Solid forms	Evaluated property	References
Nitrofurantoin	cocrystal	solubility and antimicrobial activity	[28]
Fenamic acids	salts	solubility	[29]
Malic acid	salt	solubility and antibacterial activity	[30]
Nicotinamide	salt	solubility	[31]

5.3 Results and Discussion

5.3.1 Synthesis of Molecular Salts

Six isomeric dihydroxybenzoic acids that exhibit antioxidant activities were selected as coformers based on the synthon compatibility with the drug TRM (Table 5.2). The pyrimidine···acid hydrogen-bonded heterosynthon formation is anticipated in the product materials because of the strength of donor ($O–H_{COOH}$) and acceptor ($N=C_{NCNH2}$). The OH groups in the DHBA are present to enable the manipulation of the molecular packing of the products, thereby tuning the drug properties. The multicomponent solids were synthesized using a liquid-assisted grinding method by dropwise addition of ethanol and characterized by FT-IR spectroscopy, thermal analysis, powder X-ray diffraction, and single-crystal X-ray diffraction. Among these products, three of them are in hydrated form and the remaining three are anhydrous salts. The solubility and membrane permeability measurements of all the product materials were studied in three pH conditions and compared with the pure TRM.

Table 5.2 Molecular salts of TRM with isomeric DHBAs used as coformers.

API	coformers	products	stoichiometric ratio
Trimethoprim (TRM)	2,3-Dihydroxybenzoic acid (23-DHBA)	TRM-23	1:1 TRM:23-DHBA
	2,4-Dihydroxybenzoic acid (24-DHBA)	TRM-24	1:1:2 TRM:24-DHBA:H_2O
	2,5-Dihydroxybenzoic acid (25-DHBA)	TRM-25	1:1 TRM:25-DHBA
	2,6-Dihydroxybenzoic acid (26-DHBA)	TRM-26	1:1 TRM:26-DHBA
	3,4-Dihydroxybenzoic acid (34-DHBA)	TRM-34	1:1:3 TRM:34-DHBA:H_2O
	3,5-Dihydroxybenzoic acid (35-DHBA)	TRM-35	1:1:1 TRM:35-DHBA:H_2O

5.3.2 *Characterization of product phases*

Vibrational Spectroscopy (FT-IR). Initial studies were directed to get information on whether the pure phase of the products has formed or not. FT-IR spectra of the pure TRM and its salt products with DHBAs are plotted in Figure 5.1. The N–H stretching for pure TRM occurs at 3470 and 3320 cm^{-1}, while it appears in the range 3420–3230 cm^{-1} for all products. The shifting of N–H bands in product materials indicates its involvement in hydrogen bonding with the coformers. The occurrence of an absorption band of C=O for products at a lower frequency (near 1600 and 1400 cm^{-1}) indicates the transfer of a proton from the COOH of coformers to drug TRM.

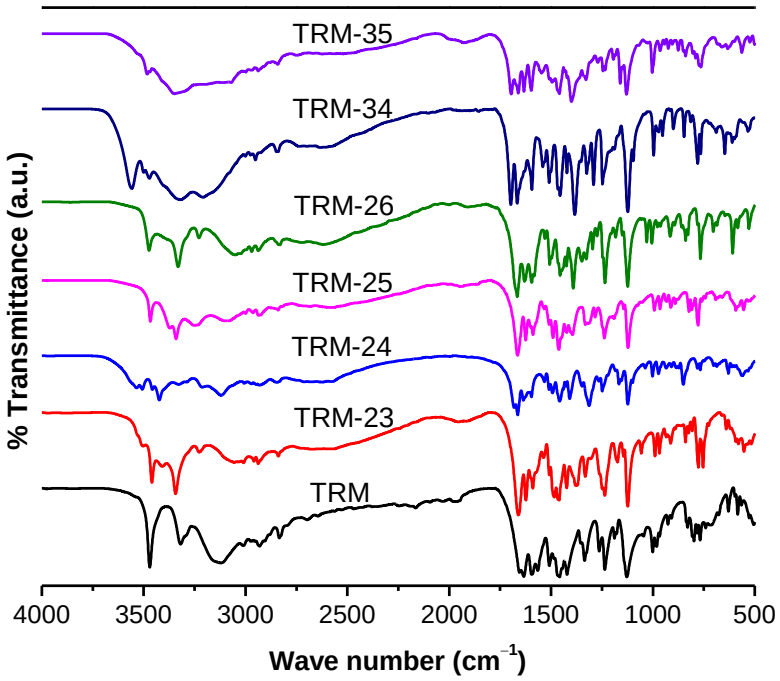

Figure 5.1 The comparison of IR spectra of TRM and its molecular salts with isomeric DHBAs.

Differential Scanning Calorimetry (DSC). The DSC analysis for all the products of TRM was performed on a Mettler Toledo DSC 822e. The thermograms obtained for the salts are plotted in Figure 5.2 and the melting point temperatures are tabulated in Table 5.3. Apart from the water loss endothermic peaks for the hydrated salts, the analysis of DSC thermograms of all product materials shows sharp melting endotherms which are different from the melting temperature of drug TRM and coformers, indicating the formation of pure single phase products. The DSC thermogram plots indicate hydrated solid formation for the products TRM-24, TRM-34, and TRM-35 as they show water loss endotherms in the temperature range of 105–135, 70–102, and 65–95 °C respectively. Meanwhile, TRM-

23, TRM-25, and TRM-26 salts are obtained as anhydrous, since no such endothermic peaks are observed in the solvent evaporation temperature range. In the case of salt TRM-35, glass transition occurs around 135 °C which signifies a transition into amorphous materials from a hard and relatively brittle glassy state into a viscous or rubbery state as the temperature is increased.

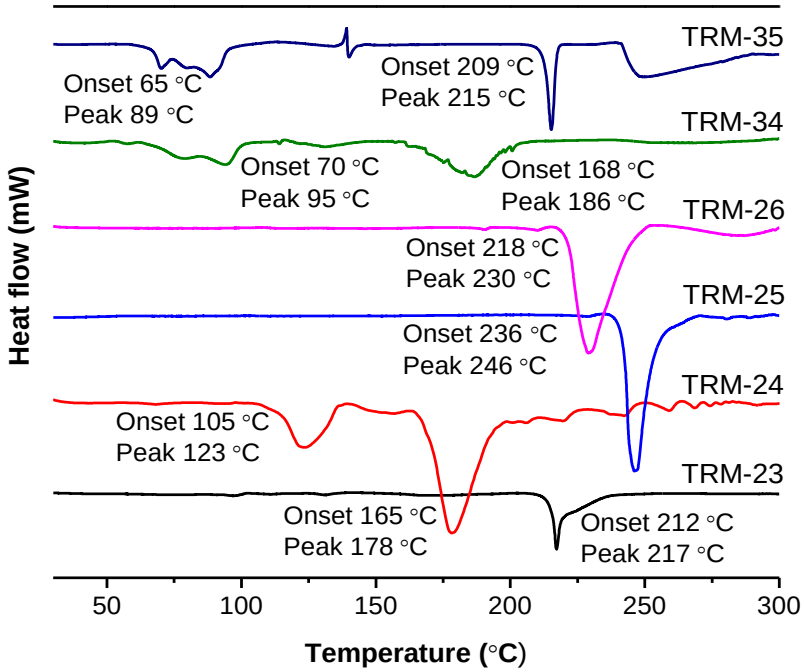

Figure 5.2 DSC endotherms represent the melting onset of the drug TRM salts.

Table 5.3 The melting onset endotherms comparison of salt products TRM-23 to TRM-35 and with their respective starting materials.

API		coformers		water loss (°C)		salts Mt. Pt. (°C)	
Mt. Pt. (°C)	coformers	Mt. Pt. (°C)	Product	onset	peak	onset	peak
	23-DHBA	204-206	TRM-23	-	-	212	217
TRM	24-DHBA	208-211	TRM-24	105	123	165	178
[198–200 °C]	25-DHBA	204–208	TRM-25	-	-	236	246
	26-DHBA	165-167	TRM-26	-	-	218	230
	34-DHBA	197-200	TRM-34	70	95	168	186
	35-DHBA	236–238	TRM-35	65	89	209	215

Thermogravimetric Analysis (TGA). The TGA also confirms the presence of water molecules of crystallization in products: TRM-24, TRM-34, and TRM-35. The water content estimated by TGA in these solids agrees well with the calculated values obtained from the single-crystal X-ray structure analysis. The TGA endotherm shows 6.63% weight loss for TRM-24 (calc. 7.49%) below 100 °C that indicates the formation of a dihydrate

structure. Similarly, trihydrate and monohydrate formation for TRM-34 (obs. 9.55% and calc. 10.83%) and TRM-35 (obs. 3.38% and calc. 3.89%) are predicted by TGA respectively (Figure 5.3). The TGA plots of the remaining products don't show water/solvent loss endotherms.

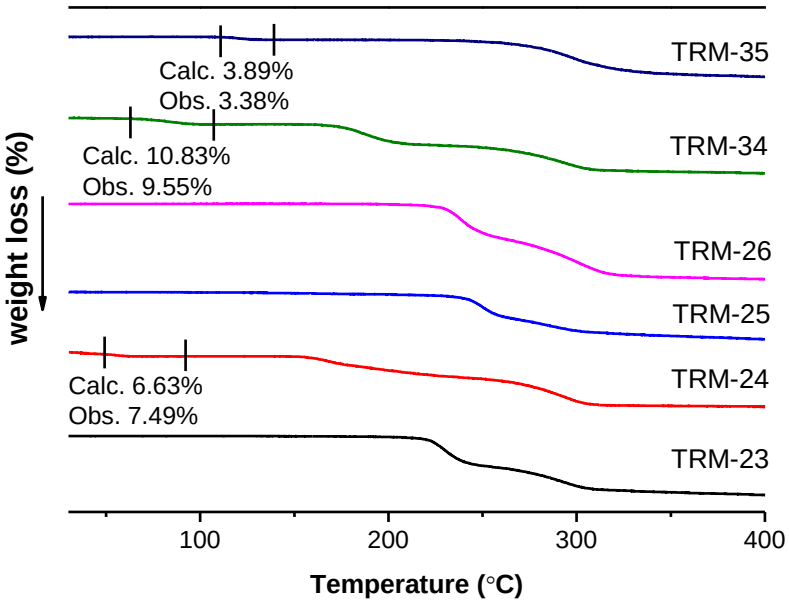

Figure 5.3 The weight loss estimated by TGA for hydrated products agrees well with the calculated values from the crystal structures.

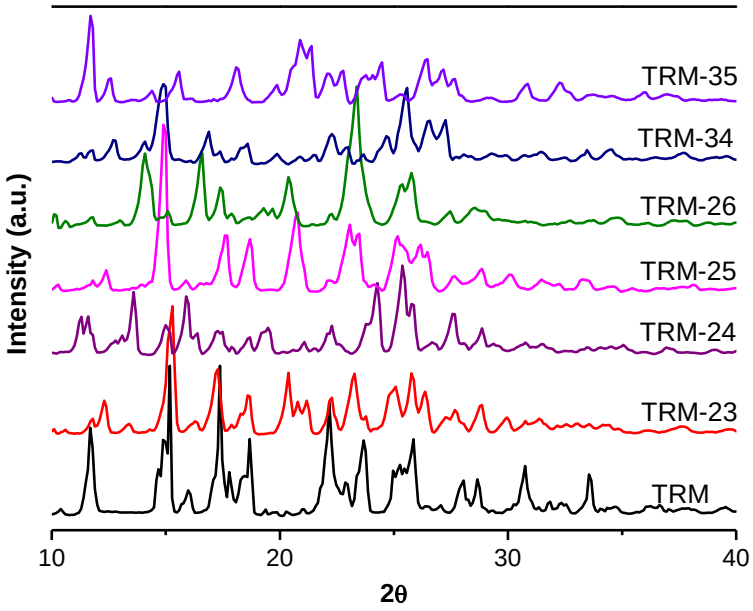

Figure 5.4 Powder X-ray diffraction patterns for salts of drug TRM with isomeric DHBA.

Powder X-ray Diffraction (PXRD). The experimental PXRD patterns of the newly synthesized materials are compared with their respective starting components (Figure 5.4).

The PXRD pattern of the products exhibits completely different phases from their respective initial components, suggesting the conversion of starting components into the new solid phase. The phase purity and homogeneity of products are evaluated by overlaying the experimental and simulated PXRD patterns of each product using Powder Cell Suite 2.3 (Appendix, Figure A6). The experimental PXRD pattern of each product material is found to be identical to the corresponding simulated pattern, specifying the phase purity of the products.

Single Crystal X-RD. The molecular interactions between the TRM and coformers are examined using single crystal X-ray diffraction. The single crystals of products for the data collection were obtained from the crystallization of ground powder materials in ethanol (EtOH) or methanol (MeOH). The formation of pyrimidinium···carboxylate supramolecular hydrogen bond heterosynthon is evident in all product structures as a prime noncovalent interaction (Figure 5.5). The proton from the COOH group is transferred to one of the basic N atoms of the pyrimidine ring. The pK_a values of starting materials and structural parameters of the acid proton in the multicomponent solids are presented in Table 5.4. The proton is located near N4 of TRM (0.88 Å) rather than the oxygen atom of DHBA (1.79–1.86 Å). Moreover, the bond angle of the N-atom of the pyrimidine (^{2}C–^{4}N–^{3}C = 115.5° for unprotonated TRM) is increased to 117.30-120.17° for the multicomponent solids suggests the formation of trimethoprim cation. The protonation of N-atom in the pyrimidine ring of the drug is due to the high difference in the pK_a value between pyrimidine and COOH groups. The protonated N-atom and NH_2 group of the trimethoprim cation are connected to the carboxylate group of DHBA via an ionic N^+–H···O^- and neutral N–H···O interactions to form an $R_2^2(8)$ ring motif. The asymmetric unit of salts TRM-23, TRM-25, and TRM-26 consists of a 1:1 ratio of the individual components, whereas TRM-24, TRM-34, and TRM-35 consist of individual components in a 1:1 ratio along with 2, 3, and 1 water molecules respectively.

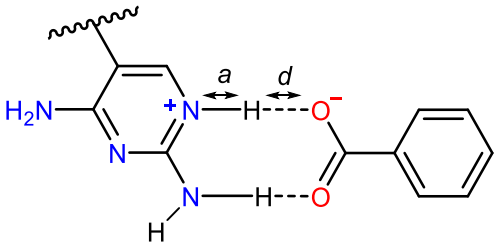

Figure 5.5 Pyrimidinium···carboxylate heterosynthon in the crystal structure of TRM salts.

Table 5.4 The pK_a values for TRM and coformers. The estimated distance parameters of COOH hydrogen atom from donor (*d*) and acceptor (*a*) atoms and N-atom bond angle parameters in the crystal structures of TRM salts (Figure 5.5).

API (pK_a)	coformers (pK_a)	acid-base ΔpK_a	product	distance (Å)		C–N–C angle (°)	solid form
				a	*d*		
TRM (7.12)	23DHBA (2.91)	4.21	TRM-23	0.88	1.80	119.22	salt
	24DHBA (3.11)	4.01	TRM-24	0.88	1.86	119.93	salt
	25DHBA (2.97)	4.15	TRM-25	0.88	1.79	120.16	salt
	26DHBA (1.51)	5.61	TRM-26	0.88	1.86	119.70	salt
	34DHBA (4.26)	2.86	TRM-34	0.88	1.86	120.17	salt
	35DHBA (4.04)	3.08	TRM-35	0.88	1.77	117.30	salt

A block-shaped crystal of TRM-24 salt dihydrate structure with a stoichiometric ratio of 1:1:2 is solved in the monoclinic $P2_1/c$ space group. Just like in the structures of other salts, a protonated TRM molecule is forming a pyrimidinium···carboxylate $R_2^2(8)$ ring motif heterodimers with a 24-DHBA molecule. An intramolecular hydrogen bonding O–H···O arises from *ortho* OH to COO^- of the DHBA molecule. Again *ortho* OH of 24-DHBA is interacting with one of the two water molecules which are connected by the O–H···O hydrogen bond while the second water molecule is forming an N–H···O and O–H···O interactions with the NH_2 group of second TRM molecule and *para* OH group of another 24-DHBA to form a 2D and 3D structure respectively (Figure 5.6a). The coformers are linked by the hydrogen bonding from the *para* OH group of 24-DHBA to the oxygen atom of the carboxylate anion of another 24-DHBA to form a one-dimensional (1D) molecular tape (Figure 5.6b).

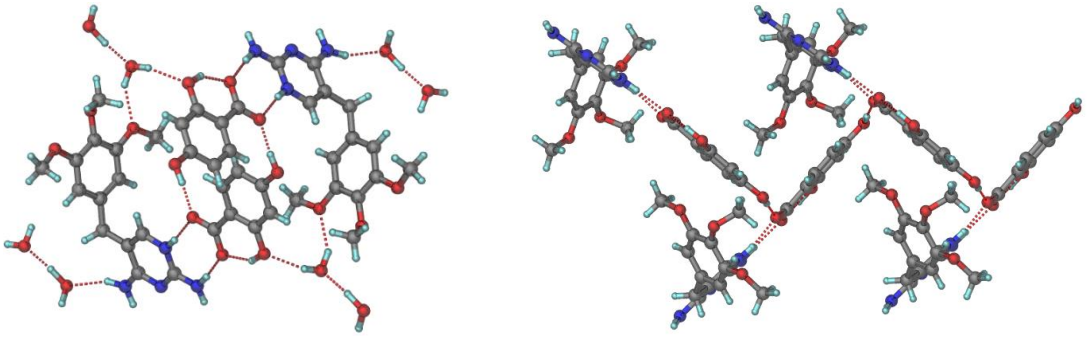

(a) (b)

Figure 5.6 (a) The water dimer extends the structure of the TRM-24 in 2D and 3D by linking the drug···coformer dimers. (b) Dimers are connected by O–H···O interaction to form a 1D layer in the crystal structure of TRM-24.

In TRM-25 salt, a needle-shaped crystal of anhydrous salt with a 1:1 stoichiometry of TRM and 25-DHBA was obtained and solved in the monoclinic system with a space group of $P2_1/n$. The COO^- of the 25-DHBA forms a heterodimer with the TRM molecule via $R_2^2(8)$ motif. Pair of such dimers, but which are arranged in an opposite direction to each other and form a molecular tape via another $R_2^2(8)$ motif (Figure 5.7a). The structure extends in 1D by hydrogen bond which is formed from the *meta* OH to *ortho* OH group of the coformer. The N–H···O hydrogen bond which is formed between the second amine group of the pyrimidine ring and ether group of TRM molecules forms sheetlike 2D layers (Figure 5.7b). The 26-DHBA coformer resulted in an anhydrous salt of drug TRM with a 1:1 stoichiometric ratio structure which is arranged in the monoclinic with *C*2/c space group. An $R_2^2(8)$ ring motif heterodimers in the crystal structure of TRM-26 are linked by N–H···O interactions between an amine group of pyridinium moiety and one of the OH group of 26-DHBA to form a molecular tape. The structure is further extended in 1D via hydrogen bonding from the second amine group of TRM to the oxygen atom of one of the ether groups in the other TRM molecule (Figure 5.7c).

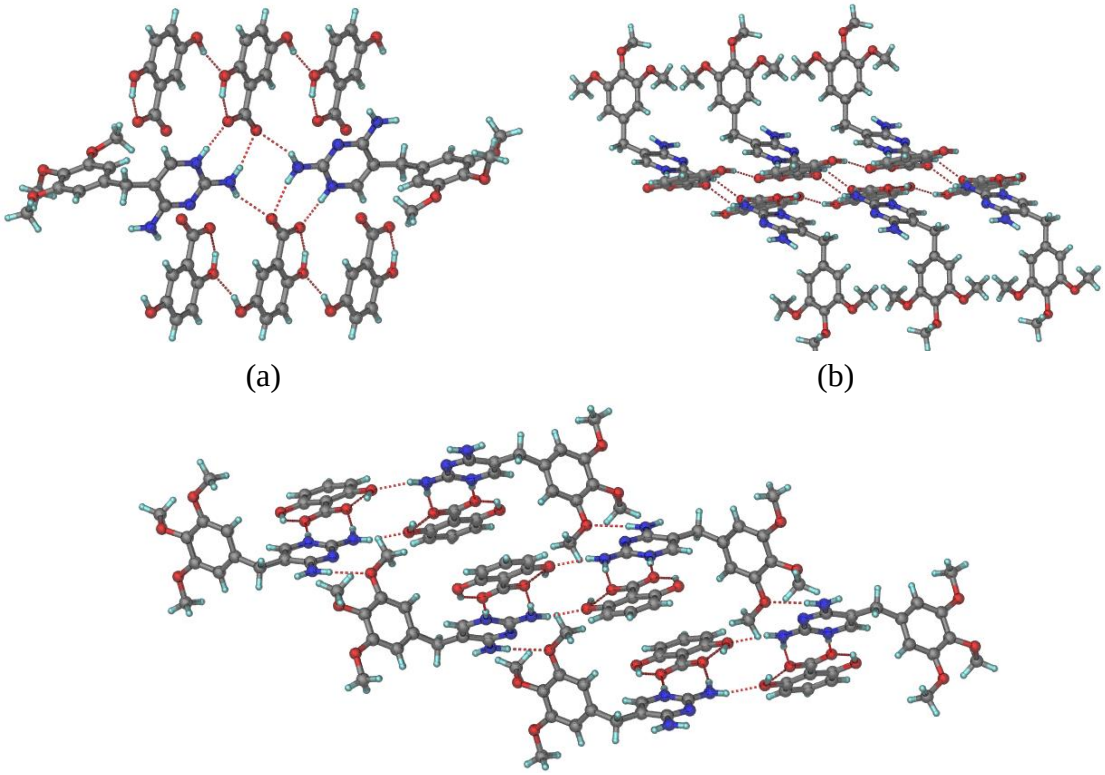

Figure 5.7 (a) Drug···coformer dimers in TRM-25 salt are connected with another $R_2^2(8)$ motif to form molecular tape. (b) 2D structure of the TRM-25 salt. (c) The molecular tapes are stacked via N–H···O interactions to complete the 1D structure of TRM-26.

The crystal structure of salt TRM-34 is solved and refined in $P\bar{1}$ space group with one TRM, one 34-DHBA, and three water molecules. Unlike the other salts of TRM, $R_2^2(8)$ motif homodimer of TRM molecules is formed in TRM-34 through N–H···N hydrogen bonding between the neutral N-atom and amine group of the pyrimidine ring. The same NH_2 group and the protonated N-atom of each TRM molecule interact with the carboxylate anion of the 34-DHBA molecule to form another $R_2^2(8)$ ring motif heterosynthon while water molecule connects the second NH_2 group of the pyrimidine ring with COO^- group of conformer. Two independent water molecules connect the *para* OH group and one of the oxygen atoms of the carboxylate anion of two inversion-related 34-DHBA molecules through a $R_2^2(20)$ ring motif via O–H···O interactions to form a molecular tape (Figure 5.8a). Water molecules also serve as a linker between ether groups of two TRM molecules through O–H···O interactions to form a netlike 2D structure supported by the hydrogen bonding from the *meta* OH group of the coformer to the oxygen atom of water molecules. Water molecules further involve in assembling netlike 2D layers of TRM-34 into the 3D structure.

A monohydrated salt structure of TRM-35 is solved in triclinic $P\bar{1}$ space group. Here like TRM-34, TRM molecules form a $R_2^2(8)$ motif homodimer through N–H···N interactions of NH_2 group and neutral N-atom of pyridinium moiety, whereas the protonated N-atom and the second NH_2 group of each TRM molecules interact with the carboxylate anion of the 35-DHBA molecule to form a heterosynthon of $R_2^2(8)$ ring motif. The 35-DHBA molecule is further connected with another inversely-related 35-DHBA molecule via water molecules through O–H···O interactions to form a cyclic $R_2^2(18)$ motif to extend the structure in a 1D (Figure 5.8b). The structure further extends in 2D by one of the OH groups of the coformer that forms a hydrogen bond with the oxygen atom of the middle ether groups of the drug to form a netlike pattern. The water molecules further involve in hydrogen bonding with the COO^- group of the coformer to form a 3D structure. The summary of single crystal data is tabulated in Appendix Table A8 and the hydrogen bond geometries of all the products are presented in Table 5.5.

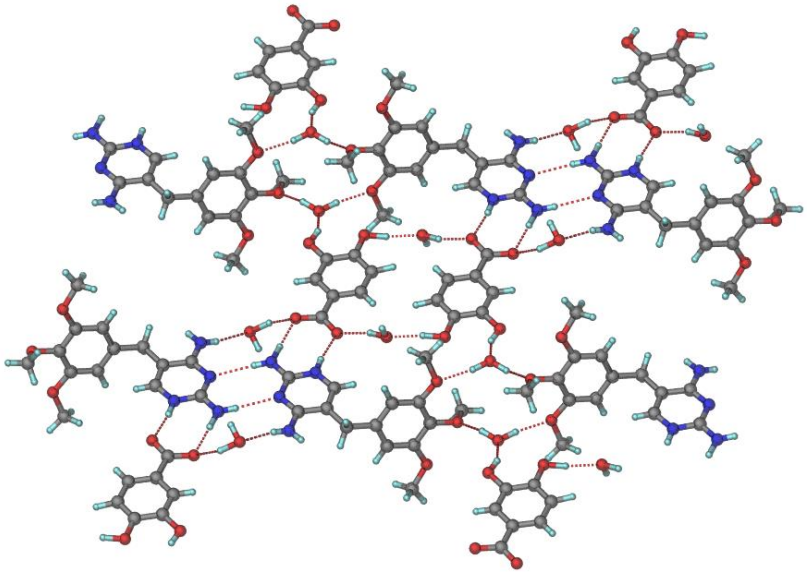

(a)

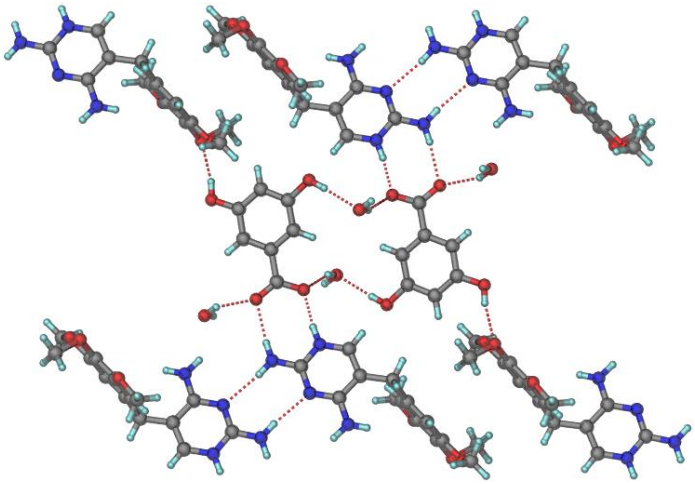

(b)

Figure 5.8 (a) The netlike 2D structure of TRM-34 is connected by N–H···O and O–H···O interactions. (b) 2D molecular packing in the crystal structure of TRM-35.

Table 5.5 Hydrogen bond parameters of salts of the drug TRM with isomeric DHBA.

salts	interactions	H···A (Å)	D···A (Å)	∠D–H···A (°)	symmetry code
TRM-24	N_3–H_{3B}···O_8	2.20	2.947(3)	145	1 + x, 1 + y, -1 + z
	N_4–H_{4A}···O_3	2.22	2.996(3)	149	1 − x, −y, 2 − z
	N_4–H_{4B}···O_5	1.97	2.829(3)	174	-
	N_3–H_{3B}···O_4	1.83	2.647(3)	174	−x, −y, −z
	N_3–H_{3B}···O_5	1.71	2.500(3)	160	1 − x, 1 − y, 1 − z
	N_3–H_{3B}···O_4	1.71	2.720(3)	170	−1/2 + x, −1/2 + y, z
TRM-25	N_3–H_1···O_5	2.35	3.026(7)	133	1 + x, 1 + y, z
	N_3–H_1···O_6	2.38	3.222(7)	158	-x, 1 - y, -z
	N_4–H_2···O_3	2.08	2.917(7)	149	1 + x, 1 + y, z

	$N_4–H_3\cdots O_3$	2.00	2.909(7)	175	x, 1 + y, z
	$O_1–H_6\cdots O_2$	1.83	2.865(7)	164	
TRM-26	$N_2–H_{2A}\cdots O_2$	1.79	2.736(3)	174	1/2 + x, 1/2 − y, 1/2 + z
	$N_3–H_{3A}\cdots O_3$	2.06	2.871(4)	150	x, 1/2 − y, 1/2 + z
	$N_3–H_{3B}\cdots O_1$	1.77	2.764(4)	172	x, 3/2 − y, 1/2 + z
	$O_1–H_{3C}\cdots O_3$	1.16	2.474(4)	150	−x, 1/2 + y, 1/2 − z
	$N_4–H_{4A}\cdots O_6$	2.21	3.102(4)	171	x, 1/2 − y, 1/2 + z
	$O_4–H_{4C}\cdots O_2$	1.62	2.566(3)	153	2 − x, 2 − y, 1 − z
TRM-34	$N_2–H_{2A}\cdots O_4$	1.78	2.736(8)	173	1 − x, −y, −z
	$N_4–H_{4A}\cdots O_5$	1.75	2.913(9)	161	−x, 1 − y, −z
	$O_{4A}–H_{4D}\cdots O_5$	1.85	2.809(8)	175	2 − x, 2 − y, 1 − z
	$O_{5A}–H_{5B}\cdots O_2$	1.89	2.857(8)	167	-
	$O_7–H_7\cdots O_{4A}$	2.07	2.893(8)	175	1 − x, 1 − y, 1 − z
	$C_{13}–H_{13B}\cdots O_3$	2.56	3.501(9)	166	
TRM-35	$O_9–H_2\cdots O_6$	1.95	2.757(5)	159	x, 3/2 − y, 1/2 + z
	$O_9–H_3\cdots O_7$	1.93	2.739(5)	157	1/2 + x, y, 1/2 − z
	$N_3–H_{3A}\cdots N_2$	2.19	3.038(4)	170	-
	$N_3–H_{3B}\cdots O_7$	2.07	2.905(4)	164	1 − x, −y, −z
	$O_4–H_{4C}\cdots O_9$	1.97	2.777(5)	167	2 − x, −1/2 + y, 1/2 − z
	$N_1–H_8\cdots O_6$	1.63	2.635(4)	174	1 − x, 1 − y, −z

5.3.3 Phase Stability Study

Multicomponent solids may undergo phase transformation or dissociation in different pH conditions during solubility and permeability evaluation. To validate the phase stability of the salt products of drug TRM, the undissolved materials (residuals) were taken from the solubility experiments in three media and studied by PXRD. A representative example of the phase stability of salt TRM-25 is demonstrated in Figure 5.9 and the remaining plots are available in Appendix Figure A7. Except for TRM-24, TRM-34, and TRM-35 at pH 1.2, the constancy of PXRD patterns for all the salt products confirms their stability up to 24 h in all three media. The undissolved sample (residual) of TRM-24 from a 1.2 pH medium shows some change in the PXRD pattern at 24 h. The prominent peaks of TRMHCl at 2θ ~13, 20, and 26° started to appear which is an indication of the phase transformation of TRM-24 into trimethoprim hydrochloride salt (Appendix Figure A7b). Similarly, the PXRD patterns of TRM-34 and TRM-35 match with that of the simulated PXRD pattern of trimethoprim hydrochloride salt signifies the conversion of these products into the trimethoprim chloride salt (Appendix Figure A8). The formation of trimethoprim chloride was also confirmed by single crystal cell check by crystallizing the aliquots after 24 h.

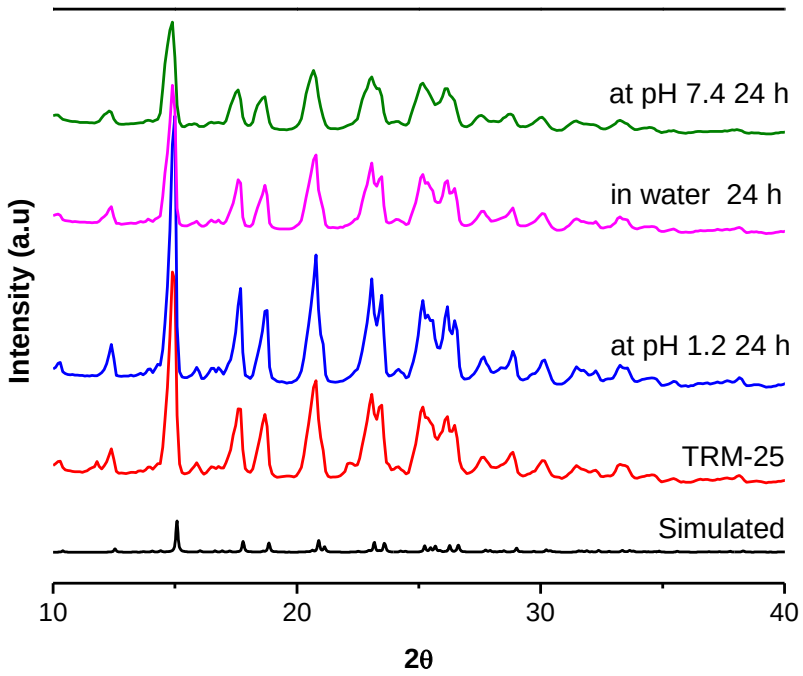

Figure 5.9 Phase stability study of TRM-25 salt of drug TRM which shows stable phase up to 24 h. The phase stability tests of the remaining products are available in Appendix Figure A7.

5.3.4 Solubility determination in various pH media

The solubility parameter of ground powder materials was evaluated in three different pH media at 24 h using UV–vis spectroscopy and the results are demonstrated in Figure 5.10 and Table 5.6. The pH change of the solutions was also recorded after the solubility experiment and didn't show a significant change. The solubility of TRM in an aqueous medium is 0.34 mg/mL which is almost similar to its reported solubility value of 0.39 mg/mL at 25 °C. All product materials display higher aqueous solubility than the pure TRM with the solubility order of TRM-35 (12.29 fold) > TRM-24 (6.18 fold) > TRM-34 (5.38 fold) > TRM-23 (2.38 fold) > TRM-26 (2.06 fold) > TRM-25 (1.29 fold). The aqueous solubility is inversely related to the melting points of the salts, except for TRM-35. The melting points order for the salts is TRM-24 (178 °C) < TRM-34 (186 °C) < TRM-35 (215 °C) < TRM-23 (217 °C) < TRM-26 (230 °C) < TRM-25 (246 °C). Thus, it is apparent from their melting points that hydrated salts have lower lattice energy than anhydrous salts, which can be the probable reason for their better aqueous solubility.

Table 5.6 Solubility amount of the TRM and its molecular salts in unit mg/mL

compound	solubility at pH 1.2	solubility in pure water	solubility at pH 7.4
TRM	8.46	0.34	0.91
TRM-23	8.92	0.81	1.02
TRM-24	21.79	2.10	1.40
TRM-25	4.93	0.44	0.76
TRM-26	4.37	0.70	1.02
TRM-34	18.61	1.83	1.86
TRM-35	18.55	4.18	2.24

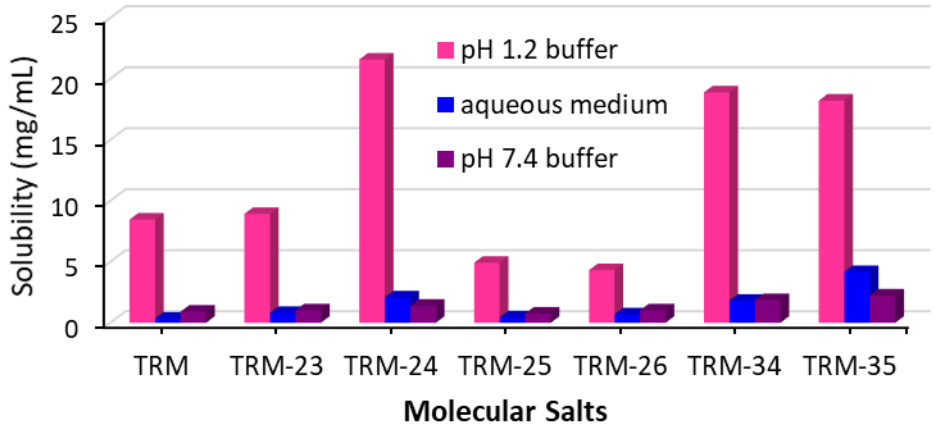

Figure 5.10 Solubility determination of the drug TRM and its molecular salts.

Similarly, hydrated salts of TRM, i.e., TRM-24 (2.57 fold), TRM-34 (2.20 fold), and TRM-35 (2.19 fold) exhibit higher improvement in the solubility at pH 1.2, whereas the anhydrous salts TRM-23 exhibits marginal improvement and TRM-25 and TRM-26 show lower solubility than the parent drug molecule. The PXRD analysis of undissolved materials taken at 24 h reveals the transformation of the three hydrated salts into trimethoprim hydrochloride salt at pH 1.2 condition (Appendix Figure A8). Apart from that it was also confirmed by the single crystal cell check by crystallizing the filtered solution of those salts at room temperature. However, the PXRD patterns of the three anhydrous salts remain unchanged for up to 24 h. The conversion of hydrated salts into trimethoprim chloride salt at pH 1.2 increases the solute···solvent interactions because of its ionic nature leading to high solubility. The solubility of the TRM salts at pH 1.2 is inversely related to the acidity of their respective coformers (see acidic strength of coformers in Table 5.4). A similar phenomenon was also reported in the cocrystals/salts of acridine with DHBAs [32]. It was also observed in molecular salts of FAM with DHBAs in Chapter 4 and the reason for such a solubility trend is discussed in section 4.3.4. At pH 7.4, enhanced solubility is observed for the hydrated salts of TRM, i.e., TRM-35 (2.46

fold), TRM-34 (2.04 fold), and TRM-24 (1.54 fold) while anhydrous salts display similar solubility with the parent API.

Hirshfeld surface analysis. In general, the presence of water molecules of crystallization in the three multicomponent solids has improved their solubility significantly in all three media. The higher solubility for the hydrated salts can be attributed to the increase in the polarity due to the water molecules of crystallization which in turn increases the solute–solvent interaction in polar media. Hirshfeld analysis of these materials shows that the polar O–H interaction for hydrated salts [TRM-24 (27.8%), TRM-34 (33.3%), TRM-35(30.3%)] is higher than that of the anhydrous salts [TRM-25 (29.6%), TRM-26) (22.1%)]. But their non-polar C–H interaction (TRM-24 (9%), TRM-34 (10%), TRM-35(12.9%)] is lower than that of the anhydrous salts [TRM-25 (12.4%), TRM-26 (14.7%)] (Figure 5.11).

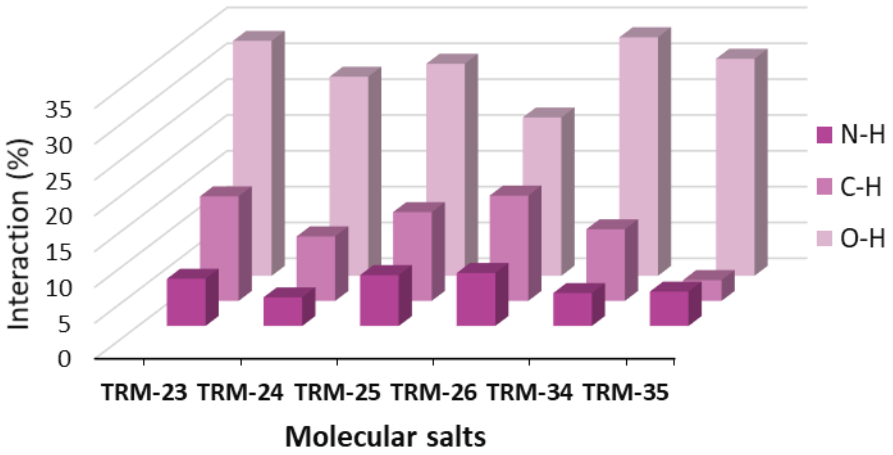

Figure 5.11 Various intermolecular interaction contributions in the molecular salts of TRM with DHBA as coformers.

5.3.5 Membrane Permeation Behaviour

The overall bioavailability of orally administrated drugs depends on the solubility and permeability across the cell membrane [33,34]. The in vitro permeation behavior of the salt products was evaluated in the saline buffer solution of pH 1.2 (Figure 5.12) and the phosphate buffer solution of pH 7.4 (Figure 5.13). The multicomponent solids demonstrated improved diffusion rate and drug flux across the cellulose membrane as compared to that of the pure TRM molecule in both media. The hydrated TRM-24, TRM-34, and TRM-35 salts display a faster release rate and drug flux than that of the anhydrous

salts TRM-23, TRM-25, and TRM-26. The hydrated salts reach a steady state at 30 min, but the anhydrous salts stay for up to 90 min.

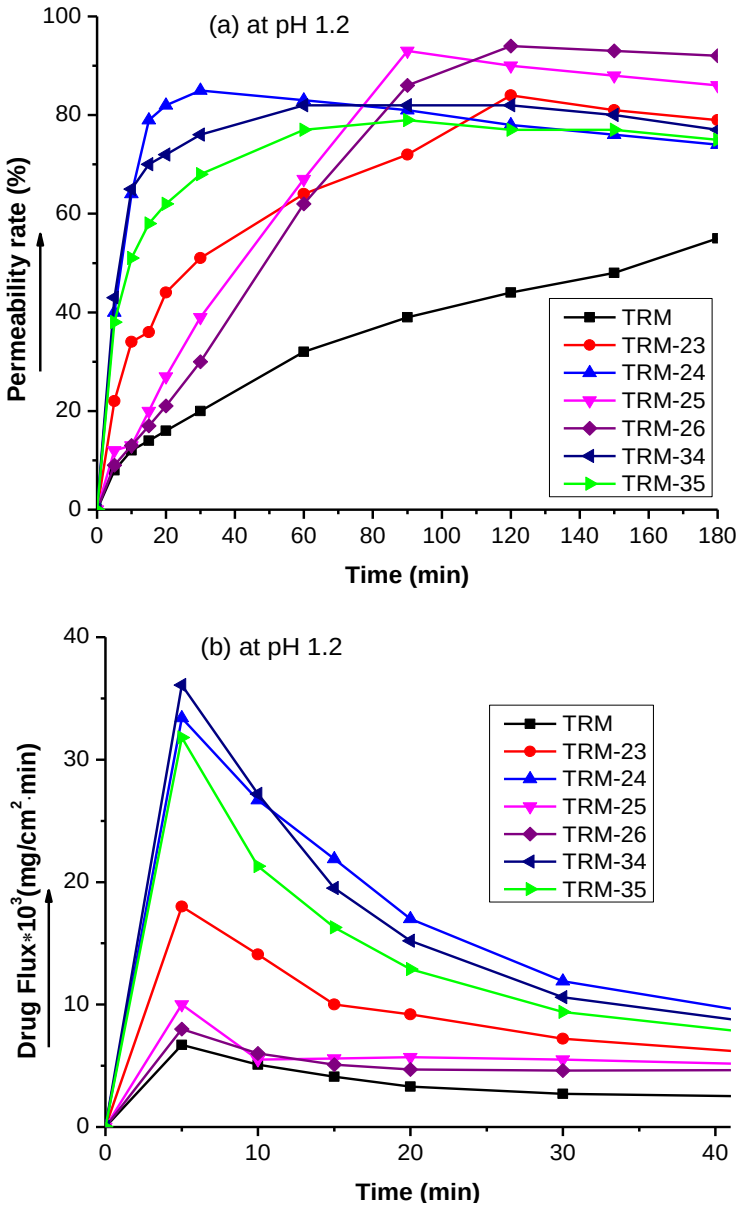

Figure 5.12 Plots of (a) membrane permeability rate and (b) drug flux of TRM and its salts with respect to time at pH 1.2.

All the salt materials and the pure API show a sharp increase in the drug flux within 5 min. The observed high permeability rate and drug flux for the hydrated salts of TRM might be because of their high solubility which causes an increase in concentration across the cellulose membrane. A similar permeability trend was observed for the famotidine salts with isomeric DHBAs in Chapter 4. A lower permeation rate was observed for the less soluble anhydrous salt of famotidine with the 26-DHBA, whereas famotidine with the rest of the DHBA coformers resulted in highly soluble and permeable hydrated salts. Desiraju

et al. formulated multicomponent solids of furosemide and hydrochlorothiazide drugs to improve their solubility and permeation properties [35,36]. They also found that multicomponent solids with high solubility displayed better membrane permeation/flux.

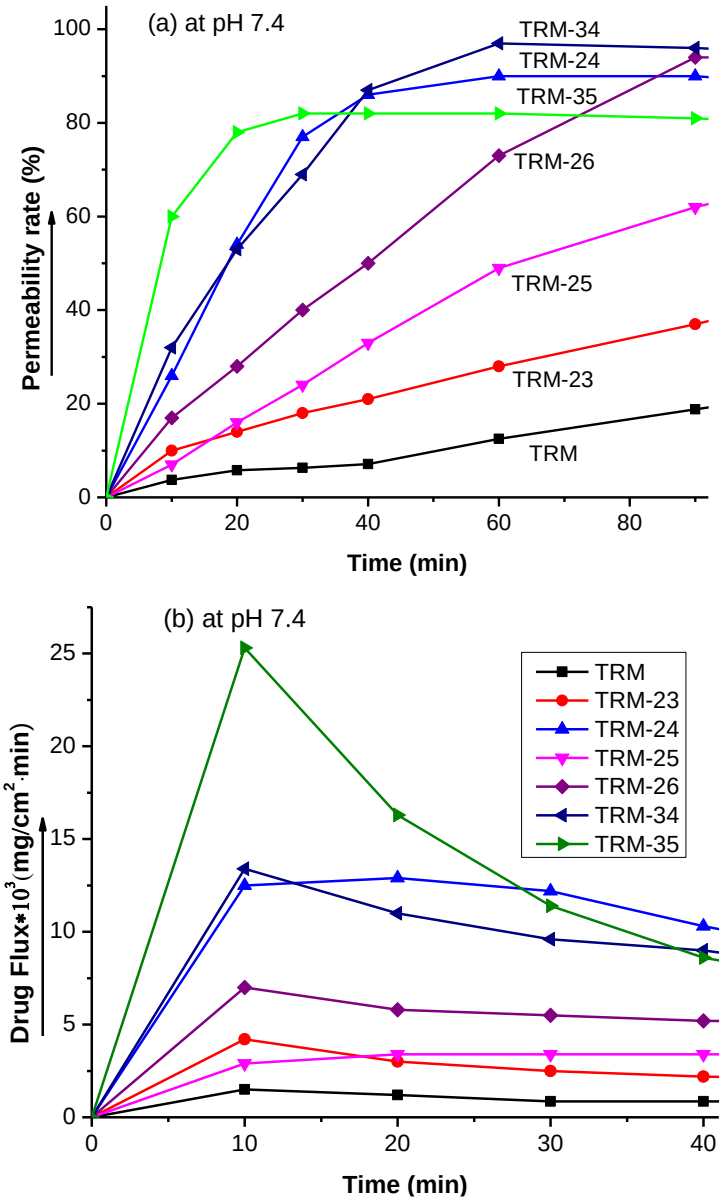

Figure 5.13 Plots of membrane permeability rate (a) and drug flux (b) of TRM and its salts with respect to time at pH 7.4.

Generally, membrane permeability depends on the lipophilic nature of the drug molecules. Compounds with high lipophilicity have a better permeation affinity. In this study, it was observed that anhydrous salts exhibit a higher lipophilicity (Figure 5.11), but display poor permeation behavior as compared to that of hydrated salts. Lipophilicity is not the only factor that determines the diffusion of drug molecules across the cell membrane. The concentration of the permeant at the absorption site which is a function of solubility also

determines its permeability through the cell membrane. Drug molecules with high solubility can have a higher concentration at the absorption site and produce higher concentration gradients over the membrane and diffuse across the membrane against lipophilicity [37].

5.4 Summary

This study aims to improve the physicochemical properties of the antibiotic drug trimethoprim by crystal engineering technique. Six pharmaceutically acceptable coformers were used to prepare molecular salts of the drug and solubility and permeation behavior were studied in three different pH conditions. These molecular salts of TRM enhanced the solubility and membrane permeation of the drug molecule. Among the products, hydrated salts, i.e., TRM-24, TRM-34, and TRM-35 showed superior solubility and permeability parameters than the anhydrous TRM-23, TRM-25, and TRM-26 salts. The enhancement of these physicochemical properties is attributed to the formation of a pyrimidinium···carboxylate heterosynthon as a main intermolecular interaction between the API and coformers, inclusion of water molecules of crystallization, and solute···solvent interactions.

5.5 Experimental Section

5.5.1 Materials

Drug trimethoprim (purity ~99%) and all the coformers were purchased from Yarrow chem products and alfa-aesar respectively and used as received. HPLC-grade solvents (methanol and ethanol) were obtained from SRL, India, and used without further purification for crystallization and grinding. Millipore water was used to carry out solubility and permeability experiments.

5.5.2 Synthesis of Molecular Salts

An equivalent stoichiometric ratio of TRM and each coformer were individually taken in a mortar and ground with a pestle for around 30 min with dropwise addition of ethanol. The ground material was transferred into a conical flask and dissolved in ethanol or methanol in ~60 °C warm condition. The solution was left for crystallization at room temperature. Suitable crystals for single crystal data collection were obtained within 3–5 days. Block-shaped crystals were obtained for the TRM-24, TRM-25, and TRM-26, whereas slightly yellowish needle-shaped transparent crystals were formed for the rest of

the products. The characterization of the obtained crystals was performed with spectroscopic, thermal, and X-ray diffraction techniques.

5.5.3 Vibrational Spectroscopy

The IR spectra of the products were recorded using a PerkinElmer Frontier spectrophotometer in the range of 400–4000 cm^{-1} (Figure 5.1). All major vibrational frequencies (in cm^{-1}) for salts are assigned as follows, TRM: 3470−3320 (N–H), 3125 (aromatic C−H), 1660 (C=N), 1596 (C=C), 1335(C−N), 1236 and 1128 (C–O); TRM-23: 3460 (OH), 3402−3227 (N−H), 3043 (aromatic C−H), 1660 (C=N), 1624 and 1371 (COO^-), 1589 (C=C), 1313 (C–N), 1236 & 1124 (C–O); TRM-24: 3505 (OH), 3420 (N–H), 3117 (aromatic C−H), 1664 (C=N), 1632 and 1409 (COO^-), 1571 (C=C), 1319 (C–N), 1249 and 1124 (C–O); TRM-25: 3470 (O–H), 3341−3247 (N–H), 3089 (aromatic C−H), 1663 (C=N), 1627 and 1394 (COO^-), 1560 (C=C), 1322 (C–N), 1239 and 1122 (C–O); TRM-26: 3474 (O–H), 3330−3230 (N–H), 3049 (aromatic C−H), 1666 (C=N), 1629 and 1391 (COO^-), 1594 (C=C), 1344 (C–N), 1236 and 1124 (C–O); TRM-34: 3558 (O–H), 3316 (N–H), 1697 (C=N), 1666 (N–H bending), 1383 (COO^-), 1594 (C=C), 1291 (C–N), 1248 and 1124 (C–O); TRM-35: 3483 (O−H), 3345 (N–H), 3070 (aromatic C−H), 1695 (C=N), 1660 (N–H bending), 1630 and 1400 (COO^-), 1597 (C=C), 1326 (C−N), 1236 and 1129 (C–O).

5.5.4 Differential Scanning Calorimetry (DSC)

Mettler Toledo DSC 822e was used to record the DSC thermograms of all the products (Figure 5.2). The melting onset temperature of the salts was compared with starting compounds in Table 5.3. The calibration of the instrument was done to check the temperature and heat flow accuracy using the melting of pure indium.

5.5.5 Thermogravimetric Analysis (TGA)

The Mettler Toledo TGA/SDTA 851e module was to analyze the quantity of solvent present in the salt materials. A sample amount of 5−10 mg was placed in the alumina pan and heated in the 30−600 °C temperature range at a rate of 10 °C/min under a dry nitrogen flow of 30 mL/min (Figure 5.3).

5.5.6 Powder X-ray Diffraction (PXRD)

PXRD of all products was recorded on a Bruker D8 Focus X-ray diffractometer, Germany using Cu-Kα X-radiation (λ = 1.54056 Å) at 35 kV and 25 mA. Diffraction patterns were collected over a 2θ range of 10–40° at a scan rate of 1° min^{-1} (Figure 5.4).

5.5.7 Single Crystal X-ray Diffraction (Single Crystal X-RD)

Bruker APEX-II CCD diffractometer was used to collect single crystal X-RD data using Mo Kα (λ = 0.71073 Å) radiation. Data reduction was done using Bruker SAINT Software. The intensity of absorption was corrected by SADABS. The crystal structure of the products was solved and refined using SHELXL with anisotropic displacement parameters for non-H atoms. The hydrogen atoms on hetero atoms were located experimentally, and C−H atoms were fixed geometrically using the HFIX command in SHELX-TL. The final CIF file checks using PLATON and didn't indicate any missed symmetry. The details of the crystallographic data of all of the products are presented in Appendix Table A8. Hydrogen bond parameters are listed in Table 5.5 and are neutron-normalized.

5.5.8 Hirshfeld Surface Analysis

The contribution percentage of various intermolecular interactions of salt hydrates was calculated using Crystal Explorer version 21 at the B3LYP/6-31G *(d, p) level of theory (Figures 5.11).

5.5.9 Solubility Measurements

The solubility of pure TRM and its salts was determined using UV–vis spectroscopy at room temperature in three different media, i.e., pH 1.2 and 7.4 buffer and aqueous medium. An excess amount of powder material of TRM and its salts was individually added to 3mL of pure water or buffer solution of pH 1.2 and 7.4 and stirred at 800 rpm rate for 24 h. The observed values were the average measurements of three for pH 1.2 and two for pH 7.4 and aqueous media. The solution was filtered and the absorbance of the aliquots was measured in an Agilent Carry-60 UV–visible double beam spectrophotometer at a room temperature of 25 °C. The concentration of an unknown solution (C_u) of the samples was calculated from the standard curves using the formula $C_u = (A_u - \text{intercept})/\text{slope}$, where A_u is the absorbance of the unknown solution.

5.5.10 Membrane Permeability Study

The permeability study of TRM and its salts was performed using a nitrocellulose membrane purchased from HiMedia, India, and a diffusion apparatus. The experiment was carried out according to the procedure reported in the literature [38,39]. A 5 mg of powder material was placed in the membrane as a donor compartment and placed in the receptor compartment with 100 mL of buffer solution (pH 1.2 or 7.4). The solution was stirred at a 700 rpm rate at a room temperature of 27 °C and allowed to diffuse via the membrane toward the receptor compartment. Three milliliters of the sample were retrieved from the receptor compartment in a definite time interval. The volume of the solution in the receptor compartment was kept constant by adding fresh solution. The amount of the compound permitted through the membrane at different time intervals was analyzed using UV–vis spectrophotometry.

5.6 References

[1] Hitching, G. H., Kuyper, L. F., and Baccananari, D. P. Design of Enzyme Inhibitors as Drugs, edited by M. Sandler & HJ Smith. *New York: Oxford University Press. N1ĐC6ĐC8*, 116(12):N1ĐC6ĐC5, 1988.

[2] Talan, D. A. New concepts in antimicrobial therapy for emergency department infections. *Annals of emergency medicine*, 34(4):503-516, 1999.

[3] Yin, D., Liu, M., Fu, H., Shu, G., Zhou, J., Qing, X., and Wu, W. Solubility of trimethoprim in selected pure solvents and (water+ ethanol/2-propanol) mixed-solvent systems. *Journal of Chemical & Engineering Data*, 61(1):404-411, 2016.

[4] Lindenberg, M., Kopp, S., and Dressman, J. B. Classification of orally administered drugs on the World Health Organization Model list of Essential Medicines according to the biopharmaceutics classification system. *European Journal of Pharmaceutics and Biopharmaceutics*, 58(2):265-278, 2004.

[5] Hetal, T., Bindesh, P., and Sneha, T. A Review on Techniques for Oral Bioavailability Enhancement of drugs. In: ; 2010.

[6] Gupta, R. L., Kumar, R., and Singla, A. K. Enhanced dissolution and absorption of trimethoprim from coprecipitates with polyethylene glycols and polyvinylpyrrolidone. *Drug development and industrial pharmacy*, 17(3):463-468,

1991.

[7] Kavanagh, O. N., Croker, D. M., Walker, G. M., and Zaworotko, M. J. Pharmaceutical cocrystals: from serendipity to design to application. *Drug Discovery Today*, 24(3):796-804, 2019.

[8] Bolla, G., Sarma, B., and Nangia, A. K. Crystal Engineering of Pharmaceutical Cocrystals in the Discovery and Development of Improved Drugs. *Chemical Reviews*, 122(13):11514–11603, 2022.

[9] Bhattacharya, S., Peraka, K. S., and Zaworotko, M. J. The role of hydrogen bonding in co-crystals. *Co-crystals: preparation, characterization and applications*, 24:33, 2018.

[10] Desiraju, G. R. Designer crystals: intermolecular interactions, network structures and supramolecular synthons. *Chemical Communications*, (16):1475-1482, 1997.

[11] Zeleke, T. Y. and Sarma, B. Isomeric Coformer Responsive Conformational Adjustment to Recuperate Stability, Solubility, and In Vitro Permeation Behavior of Drug Molecular Salts. *Crystal Growth & Design*, 22(12):7405–7418, 2022.

[12] Chennuru, R., Devarapalli, R., Rengaraj, P., Srinivas, P. L., Dey, S., and Reddy, C. M. Improving solubility of poorly soluble abiraterone acetate by cocrystal design aided by in silico screening. *Crystal Growth & Design*, 20(8):5018-5030, 2020.

[13] Yu, Q., Yan, Z., Bao, J., Wang, J.-R., and Mei, X. Taming photo-induced oxidation degradation of dihydropyridine drugs through cocrystallization. *Chemical Communications*, 53(91):12266-12269, 2017.

[14] Song, L., Robeyns, K., Tumanov, N., Wouters, J., and Leyssens, T. Combining API in a dual-drug ternary cocrystal approach. *Chemical Communications*, 56(86):13229-13232, 2020.

[15] Saikia, B., Sultana, N., Kaushik, T., and Sarma, B. Engineering a Remedy to Improve Phase Stability of Famotidine under Physiological pH Environments. *Crystal Growth and Design*, 19(11):6472-6481, 2019.

[16] Mannava, M. K. C., Bommaka, M. K., Dandela, R., Solomon, K. A., and Nangia, A. K. Fluorobenzoic acid coformers to improve the solubility and permeability of

the BCS class IV drug naftopidil. *Chemical Communications*, 58(37):5582-5585, 2022.

[17] Smith, A. J., Kavuru, P., Wojtas, L., Zaworotko, M. J., and Shytle, R. D. Cocrystals of quercetin with improved solubility and oral bioavailability. *Molecular pharmaceutics*, 8(5):1867-1876, 2011.

[18] Khatioda, R., Saikia, B., Das, P. J., and Sarma, B. Solubility and in vitro drug permeation behavior of ethenzamide cocrystals regulated in physiological pH environments. *CrystEngComm*, 19(46):6992-7000, 2017.

[19] Wang, X., Wang, L., Yao, C., Xie, G., Song, S., Li, H., Qu, Y., and Tao, X. Novel Formulations of the Antiviral Drug Favipiravir: Improving Permeability and Tabletability. *Crystal Growth & Design*, 21(7):3807-3817, 2021.

[20] Nakai, H., Takasuka, M., and Shiro, M. X-Ray and infrared spectral studies of the ionic structure of trimethoprim–sulfamethoxazole 1: 1 molecular complex. *Journal of the Chemical Society, Perkin Transactions 2*, (9):1459-1464, 1984.

[21] Bettinetti, G. and Sardone, N. Methanol solvate of the 1: 1 molecular complex of trimethoprim and sulfadimidine. *Acta Crystallographica Section C: Crystal Structure Communications*, 53(5):594-597, 1997.

[22] Alaa Eldin Refat, L., O'Malley, C., Simmie, J. M., McArdle, P., and Erxleben, A. Differences in Coformer Interactions of the 2,4-Diaminopyrimidines Pyrimethamine and Trimethoprim. *Crystal Growth & Design*, 22(5):3163-3173, 2022.

[23] Prabakaran, P., Robert, J. J., Thomas Muthiah, P., Bocelli, G., and Righi, L. Aminopyrimidine–carboxyl (ate) interactions in trimethoprim maleate, an antifolate drug. *Acta Crystallographica Section C: Crystal Structure Communications*, 57(4):459-461, 2001.

[24] Raj, S. B., Muthiah, P. T., Rychlewska, U., and Warzajtis, B. Pseudo-polymorphism and crystal engineering: hydrogen-bonded supramolecular networks in trimethoprim m-chlorobenzoate and trimethoprim m-chlorobenzoate dihydrate. *CrystEngComm*, 5(9):48-53, 2003.

[25] Subashini, A., Samuel, E., Muthiah, P. T., Bocelli, G., and Cantoni, A.

Trimethoprimium 3, 5-dinitrosalicylate. *Acta Crystallographica Section E: Structure Reports Online*, 63(10):4049-4049, 2007.

[26] Hemamalini, M., Muthiah, P. T., and Lynch, D. E. Hydrogen-bonding patterns in trimethoprim picolinate and 2-amino-4, 6-dimethylpyrimidinium picolinate hemihydrate. *Acta Crystallographica Section C: Crystal Structure Communications*, 62(2):107-110, 2006.

[27] Ton, Q. C. and Egert, E. Cocrystals of the antibiotic trimethoprim with glutarimide and 3, 3-dimethylglutarimide held together by three hydrogen bonds. *Acta Crystallographica Section C: Structural Chemistry*, 71(1):75-79, 2015.

[28] Maity, D. K., Paul, R. K., and Desiraju, G. R. Drug–drug binary solids of nitrofurantoin and trimethoprim: crystal engineering and pharmaceutical properties. *Molecular Pharmaceutics*, 17(12):4435-4442, 2020.

[29] Bhattacharya, B., Das, S., Lal, G., Soni, S. R., Ghosh, A., Reddy, C. M., and Ghosh, S. Screening, crystal structures and solubility studies of a series of multidrug salt hydrates and cocrystals of fenamic acids with trimethoprim and sulfamethazine. *Journal of Molecular Structure*, 1199:127028, 2020.

[30] Yuliandra, Y., Hutabarat, L. J., Ardila, R., Octavia, M. D., and Zaini, E. Enhancing solubility and antibacterial activity using multicomponent crystals of trimethoprim and malic acid. *Pharm Educ*, 21(2):296-304, 2021.

[31] Zheng, Q., Unruh, D. K., and Hutchins, K. M. Cocrystallization of trimethoprim and solubility enhancement via salt formation. *Crystal Growth & Design*, 21(3):1507-1517, 2021.

[32] Bora, P., Saikia, B., and Sarma, B. Regulation of π···π Stacking Interactions in Small Molecule Cocrystals and/or Salts for Physiochemical Property Modulation. *Crystal Growth & Design*, 18(3):1448-1458, 2018.

[33] Amidon, G. L., Lennernäs, H., Shah, V. P., and Crison, J. R. A theoretical basis for a biopharmaceutic drug classification: the correlation of in vitro drug product dissolution and in vivo bioavailability. *Pharmaceutical research*, 12(3):413-420, 1995.

[34] Lipinski, C. A., Lombardo, F., Dominy, B. W., and Feeney, P. J. Experimental and

computational approaches to estimate solubility and permeability in drug discovery and development settings. *Advanced drug delivery reviews*, 23(1-3):3-25, 1997.

[35] Banik, M., Gopi, S. P., Ganguly, S., and Desiraju, G. R. Cocrystal and salt forms of furosemide: solubility and diffusion variations. *Crystal Growth & Design*, 16(9):5418-5428, 2016.

[36] Gopi, S. P., Banik, M., and Desiraju, G. R. New cocrystals of hydrochlorothiazide: optimizing solubility and membrane diffusivity. *Crystal Growth & Design*, 17(1):308-316, 2017.

[37] Lipinski, C. A., Lombardo, F., Dominy, B. W., and Feeney, P. J. Experimental and computational approaches to estimate solubility and permeability in drug discovery and development settings. *Advanced drug delivery reviews*, 46(1-3):3-26, 2001.

[38] Sanphui, P., Devi, V. K., Clara, D., Malviya, N., Ganguly, S., and Desiraju, G. R. Cocrystals of Hydrochlorothiazide: Solubility and Diffusion/Permeability Enhancements through Drug–Coformer Interactions. *Molecular Pharmaceutics*, 12(5):1615-1622, 2015.

[39] Saikia, B., Bora, P., Khatioda, R., and Sarma, B. Hydrogen Bond Synthons in the Interplay of Solubility and Membrane Permeability/Diffusion in Variable Stoichiometry Drug Cocrystals. *Crystal Growth and Design*, 15(11):5593-5603, 2015.